

Spora: A Journal of Biomathematics

Volume 3 | Issue 1

Article 4

2017

Modeling Aggregation of Proliferating Microglia in Response to Amyloid-beta in Dementia


Adrienne C. Kinney

Centre College, ackinney1@gmail.com

Ellen R. Swanson

Centre College, ellen.swanson@centre.edu

Follow this and additional works at: <https://ir.library.illinoisstate.edu/spora>

 Part of the [Other Applied Mathematics Commons](#), and the [Other Neuroscience and Neurobiology Commons](#)

Recommended Citation

Kinney, Adrienne C. and Swanson, Ellen R. (2017) "Modeling Aggregation of Proliferating Microglia in Response to Amyloid-beta in Dementia," *Spora: A Journal of Biomathematics*: Vol. 3: Iss.1, .

DOI: <http://doi.org/10.30707/SPORA3.1Kinney>

Available at: <https://ir.library.illinoisstate.edu/spora/vol3/iss1/4>

This Mathematics Research is brought to you for free and open access by ISU ReD: Research and eData. It has been accepted for inclusion in Spora: A Journal of Biomathematics by an authorized editor of ISU ReD: Research and eData. For more information, please contact ISURed@ilstu.edu.

Modeling Aggregation of Proliferating Microglia in Response to Amyloid-beta in Dementia

Cover Page Footnote

The authors would like to thank Abby Quirk-Royal for her helpful discussions and suggestions.

Modeling Aggregation of Proliferating Microglia in Response to Amyloid- β in Dementia

Adrienne C. Kinney¹, Ellen R. Swanson^{1,*}

*Correspondence:
Prof. Ellen R Swanson, Dept.
of Mathematics, Centre
College, 600 W. Walnut St.
Danville, KY 40422, USA
ellen.swanson@centre.edu

Abstract

Amyloid-beta plaques are prominent biological markers in dementia brains. In response to plaque formation, the brain's immune cells, microglia, become reactive. Microglia are measurable cells that surround amyloid-beta plaques, indicating their location. A system of partial differential equations describes the concentration of microglia in dementia brains by incorporating chemotactic signaling. However, this system fails to incorporate increasing numbers of reactive microglia cells in response to amyloid-beta aggregation. A system of ordinary differential equations describing the number of significant cells and proteins in the brain suggests the amount of reactive microglia increases significantly during the progression of dementia. We couple these two systems to examine the influence of increasing amounts of reactive microglia on microglia concentration, which is indicative of amyloid-beta plaques. We compare the results of these systems to data and confirm the ability to predict the width of the aggregated microglia clusters when increasing amounts of microglia are included.

Keywords: dementia pathogenesis model, microglia proliferation, amyloid-beta plaque development, numerical simulations

1 Introduction

Dementia is a degenerative brain disorder causing neuron connections to deteriorate within the brain and the eventual death of neurons [1]. The pathogenesis of two common forms of dementia, Alzheimer's Disease (AD) and Parkinsonian Dementia (PD), is categorized by characteristic amyloid-beta ($A\beta$) protein plaque development [13, 8]. Throughout the progression of AD and PD, $A\beta$ aggregates into destructive plaques, altering the cell makeup of the brain [12]; however, symptomatic onset frequently occurs 17 years after the initial presence of the disease [29].

Dementia pathogenesis focuses on two proteins: $A\beta$ protein and tau protein [1]. Amyloid-beta proteins, $A\beta$ aggregate and form dense plaques that are toxic to neurons and inhibit neuron synapses, during the progression of the disease [12]. In a healthy brain, tau proteins stabilize microtubules, which run throughout a neuron and transport nutrients. Throughout dementia progression, however, tau proteins misfold and fall off microtubules, causing the microtubules to disintegrate and leading to eventual cell death [3]. While the disintegration of τ -proteins play a key role in the progression of dementia, we focus on the impacts of $A\beta$.

The aggregation of $A\beta$ coincides with notable changes

in composition of cells in a dementia brain. Healthy brains are composed of glial cells and neurons. Neurons transmit information throughout the brain and glial cells provide support and protection for neurons [12]. Microglia and astrocytes, subcategories of glial cells, are impacted during the degradation of neurons due to $A\beta$. In a healthy brain, astrocytes regulate synapses among neurons and are quiescent [6, 28]. Astrocytes proliferate throughout disease progression [23, 12]. Microglial cells are the immune response cells [27] and exhibit chemotactic behavior [16, 26, 18, 25], meaning that chemicals functioning either as a chemoattractant or chemorepellent are excreted either by or in response to the microglia cells. When a foreign substance enters the brain, microglia cells sensing the substance excrete a chemoattractant, resulting in the migration of other microglial cells towards the foreign substance [4, 21, 22]. Once the foreign substance is surrounded, the microglia revert to a reactive state, and in this state are able to remove the foreign substance [12]. As $A\beta$ aggregate into plaques in a dementia brain, microglia become reactive and surround the plaques, yet are unsuccessful in removing the plaques. The unimpeded aggregation of $A\beta$ is believed to worsen the symptoms of dementia [10, 24]. The progression of dementia, particularly the aggregation of $A\beta$, causes large amounts of normal microglia to revert to their reactive state and form dense clusters around $A\beta$ plaques [11].

Luca et. al. [15] create a system of partial differen-

¹Department of Mathematics, Centre College, Danville, KY

tial equations to model the distribution of microglia in response to chemoattractant and repellents, specifically IL-1 β and TNF- α . This system solely examines the relationship between the reactive microglia and the chemoattractants and repellents. Edelstein-Keshet et. al. [5] computationally examine the roles of neurons, cytokines, astrocytes, microglia, and A β in the formation of plaques. However, both of these studies assume a constant amount of reactive microglia. Puri et. al. [23] describe the cross-talk between microglia, astrocytes, neurons, and A β through a system of ordinary differential equations. These results suggest a substantial increase in the proliferation of reactive microglia during the progression of dementia.

In this paper, we focus on incorporating an increasing amount of reactive microglia to better understand the movement of microglia and its connection to A β plaques. In §2 we outline the chemotaxis model presented in [15] and compare the results to data from a Parkinsonian Dementia patient [17]. In §3 we outline the proliferation model presented in [23] for the amounts of relevant types of cells and proteins. In §4 we couple the models, developing a chemotaxis model with proliferation and compare the results to both the original chemotaxis model and data of microglia clusters from a Parkinsonian Dementia patient [17]. While we acknowledge a difference in the pathogenesis of Parkinsonian Dementia and Alzheimer’s Disease, both diseases feature the aggregation of A β plaques [1], and we assume microglia react to A β aggregation similarly in AD and PD. Thus, we present the chemotaxis model with proliferation used to describe microglia behavior in dementia brains, and use data from a PD brain to verify the model.

2 Chemotaxis Model

Luca et. al. [15] describe the concentration, in 1 dimension, of reactive microglia cells over time and space, and is founded on the assumption that microglia are chemotactic cells. The authors identify IL-1 β as a chemoattractant and TNF- α as a chemorepellent. When IL-1 β is secreted, microglial cells are estimated to move towards the chemical at a rate of 1–2 $\mu\text{m min}^{-1}$, and when TNF- α is secreted the microglia are estimated to move at the same rate away from the chemical [7]. The chemoattractant and chemorepellent used in the model are implicated in AD and are known to induce microglial movement [14, 16, 26, 19, 25].

The chemotaxis model (1) predicts the concentration of microglia in response to arbitrary initial concentrations of the chemoattractant and chemorepellent. The model is a coupled system of partial differential equations, where the variable m is the concentration of reactive microglia, c_1

is the concentration of the chemoattractant, IL-1 β , and c_2 is the concentration of the chemorepellent, TNF- α .

$$\frac{\partial m}{\partial t} = \mu \frac{\partial^2 m}{\partial x^2} - \frac{\partial}{\partial x} \left(\chi_1 m \frac{\partial c_1}{\partial x} - \chi_2 m \frac{\partial c_2}{\partial x} \right), \quad (1a)$$

$$\frac{\partial c_1}{\partial t} = D_1 \frac{\partial^2 c_1}{\partial x^2} + a_1 m - b_1 c_1, \quad (1b)$$

$$\frac{\partial c_2}{\partial t} = D_2 \frac{\partial^2 c_2}{\partial x^2} + a_2 m - b_2 c_2 \quad (1c)$$

The parameters used in the model (1) are defined in Table 1.

Variable	Description	Value
μ	Microglia random motility	33 $\mu\text{m}^2 \text{min}^{-1}$
χ_1	Chemoattraction	6–780 $\mu\text{m}^2 \text{nM}^{-1} \text{min}^{-1}$
χ_2	Chemorepulsion	Not provided
D_1	IL-1 β diffusion	900 $\mu\text{m}^2 \text{min}^{-1}$
D_2	TNF- α diffusion	900 $\mu\text{m}^2 \text{min}^{-1}$
a_1	IL-1 β production rate	$6.25 * 10^{-6} \text{pg min}^{-1}$
a_2	TNF- α production rate	$8.33 * 10^{-6} \text{pg min}^{-1}$
b_1	IL-1 β decay rate	0.003–0.03 min^{-1}
b_2	TNF- α decay rate	0.002–0.03 min^{-1}
\bar{m}	Average cell density	10^{-6} – 10^{-4} cells μm^{-3}

Table 1: Parameters for the chemotaxis model (1) from [15]

Using the dimensionless variables

$$x^* = \frac{x}{\hat{x}}, \quad t^* = \frac{t}{\hat{t}}, \quad m^* = \frac{m}{\hat{m}}, \quad c_1^* = \frac{c_1}{\hat{c}_1}, \quad c_2^* = \frac{c_2}{\hat{c}_2} \quad (2)$$

where L_1 and L_2 are the spatial ranges for the chemoattractant and chemorepellent, τ is used as the time scale, and

$$\hat{x} = L_2 = \sqrt{D_2/b_2}, \quad \hat{t} = \tau = L_2^2/\mu, \quad \hat{m} = \bar{m} \\ \hat{c}_1 = a_1 \bar{m}/b_1, \quad \hat{c}_2 = a_2 \bar{m}/b_2,$$

we create the nondimensional system, dropping the stars,

$$\frac{\partial m}{\partial t} = \frac{\partial^2 m}{\partial x^2} - \frac{\partial}{\partial x} \left[\left(A_1 \frac{\partial c_1}{\partial x} - A_2 \frac{\partial c_2}{\partial x} \right) m \right] \quad (3a)$$

$$\epsilon_1 \frac{\partial c_1}{\partial t} = \frac{\partial^2 c_1}{\partial x^2} + a^2(m - c_1) \quad (3b)$$

$$\epsilon_2 \frac{\partial c_2}{\partial t} = \frac{\partial^2 c_2}{\partial x^2} + m - c_2. \quad (3c)$$

The dimensionless parameters are

$$A_1 = \frac{\chi_1 a_1 \bar{m}}{\mu b_1}, \quad A_2 = \frac{\chi_2 a_2 \bar{m}}{\mu b_2}, \quad \epsilon_1 = \frac{\mu}{D_1},$$

$$\epsilon_2 = \frac{\mu}{D_2}, \quad a = \frac{L_2}{L_1}, \quad A = \frac{\chi_1 a_1 D_2}{\chi_2 a_2 D_1}$$

and the values are in Table 2.

Parameter	A_1	A_2	ϵ_1	ϵ_2
Value	37.50	100	0.0367	0.0367
Parameter	a	A	xLen	
Value	2	1.5	5	

Table 2: Dimensionless parameter values used in the chemotaxis model (3) from [15]

We use random initial conditions for the densities of m , c_1 , and c_2 obtained using (4),

$$m(x, 0) = 1 + \epsilon * x1_{ran} \quad (4a)$$

$$c_1(x, 0) = 1 + \epsilon * x2_{ran} \quad (4b)$$

$$c_2(x, 0) = 1 + \epsilon * x3_{ran} \quad (4c)$$

where $\epsilon = 0.002$ and $x_{i_{ran}}$ is a uniform random variable such that $|x_{i_{ran}}| < 1$. Note $x_{i_{ran}}$ is a different distribution for each initial density.

We assume no-flux boundary conditions

$$\mu \frac{\partial m}{\partial x} - \left(\chi_1 m \frac{\partial c_1}{\partial x} - \chi_2 m \frac{\partial c_2}{\partial x} \right) \Big|_{x=0, xLen} = 0 \quad (5a)$$

$$\frac{\partial c_1}{\partial x} \Big|_{x=0, xLen} = 0 \quad (5b)$$

$$\frac{\partial c_2}{\partial x} \Big|_{x=0, xLen} = 0. \quad (5c)$$

We solve the chemotaxis model (3) using the PDEPE solver in MATLAB over the nondimensional length of the strip of brain $xLen$, where the initial condition is shown in Figure 1a. The concentrations of reactive microglia, chemoattractant, and chemorepellent at $t = 0.03$, $t = 0.25$, and $t = 0.70$, for $xLen = 5$, are shown in Figure 1b–d. The red lines in Figure 1 represent reactive microglia concentration, the blue lines represent chemoattractant (IL-1 β) concentration, and the green lines represent chemorepellent (TNF- α) concentration. Over time, distinct clusters of reactive microglial cells form. The chemotaxis behavior of microglia is triggered by the presence of foreign substances, and in dementia the triggering foreign substance may be A β [9]. As a result, the concentration of microglia in a dementia brain will be densest surrounding A β plaques. The clusters observed in Figure 1 are thus indicative of A β plaques. Luca et. al. [15]

performed a stability analysis of this model and determined the number of peaks for $xLen = 5$ are dependent on the parameters in the model. Considering a larger value of $xLen$ results in a greater number of peaks. For $xLen = 5$ and using the parameters defined in Table 2, three peaks form regardless of the initial condition, consistent with [15]. The initial distributions of chemoattractant and chemorepellent used in Figure 1b–d resulted in decreasing magnitudes of the microglia clusters, however; varying distributions of chemoattractant and chemorepellent will change the microglia cluster magnitudes, yielding potentially different patterns of peak formation than observed in Figure 1b–d.

We compare the results of the chemotaxis model (1) to an image of stained reactive microglia cells in the brain of a deceased Parkinsonian Dementia patient [17], again assuming microglia behavior in PD brains is representative of all dementia patients suffering from PD and AD [1]. We use an image of stained reactive microglial cells from the hippocampus of a PD brain (Figure 4 from [17]). The image shows a section of the brain $10^4 \mu\text{m}^2$ in area and $30 \mu\text{m}$ thick [15]. Since we are considering a 1-dimensional strip of the brain, we work with a strip 2cm above the bottom of the image and spanning the width of the image. Using the IMPROFILE function in MATLAB, we determine the intensity values of the pixels along this chosen line on the image in grayscale. The intensity values of the pixels increase as the density of reactive microglial cells increase. However, we focus on comparing the spatial width of the predicted microglia clusters rather than the concentration amount, due to the unavailability of the necessary information to calibrate the image to determine the actual concentration of microglia. We determine the spatial width of the microglial clusters in a PD brain by nondimensionalizing the width of the image, using \hat{x} , and examining the profile of the pixel values. We normalize the pixel intensities to the maximum and minimum value of the microglia concentrations predicted by the chemotaxis model (3), and overlay the pixel intensity profile on the same nondimensionalized spatial scale as used by the chemotaxis model (3). The maximum and minimum values used to nondimensionalize the data vary with each set of initial conditions, since the initial conditions are randomly generated.

Figure 2 shows the predicted concentration of microglia from the chemotaxis model at $t = 0.10$ compared to the data for reactive microglia cells in a PD brain. The value $t = 0.10$ corresponds to about 18 years, and we consider the results at this time to allow for sufficient disease progression. The peak of the pixel intensity profile in Figure 2 corresponds to the high density microglia cluster observed in Figure 4 from [17]. The nondimensionalized width of the pixel intensity profile obtained from Figure 4 of [17] is less than 0.5 units; however, we display

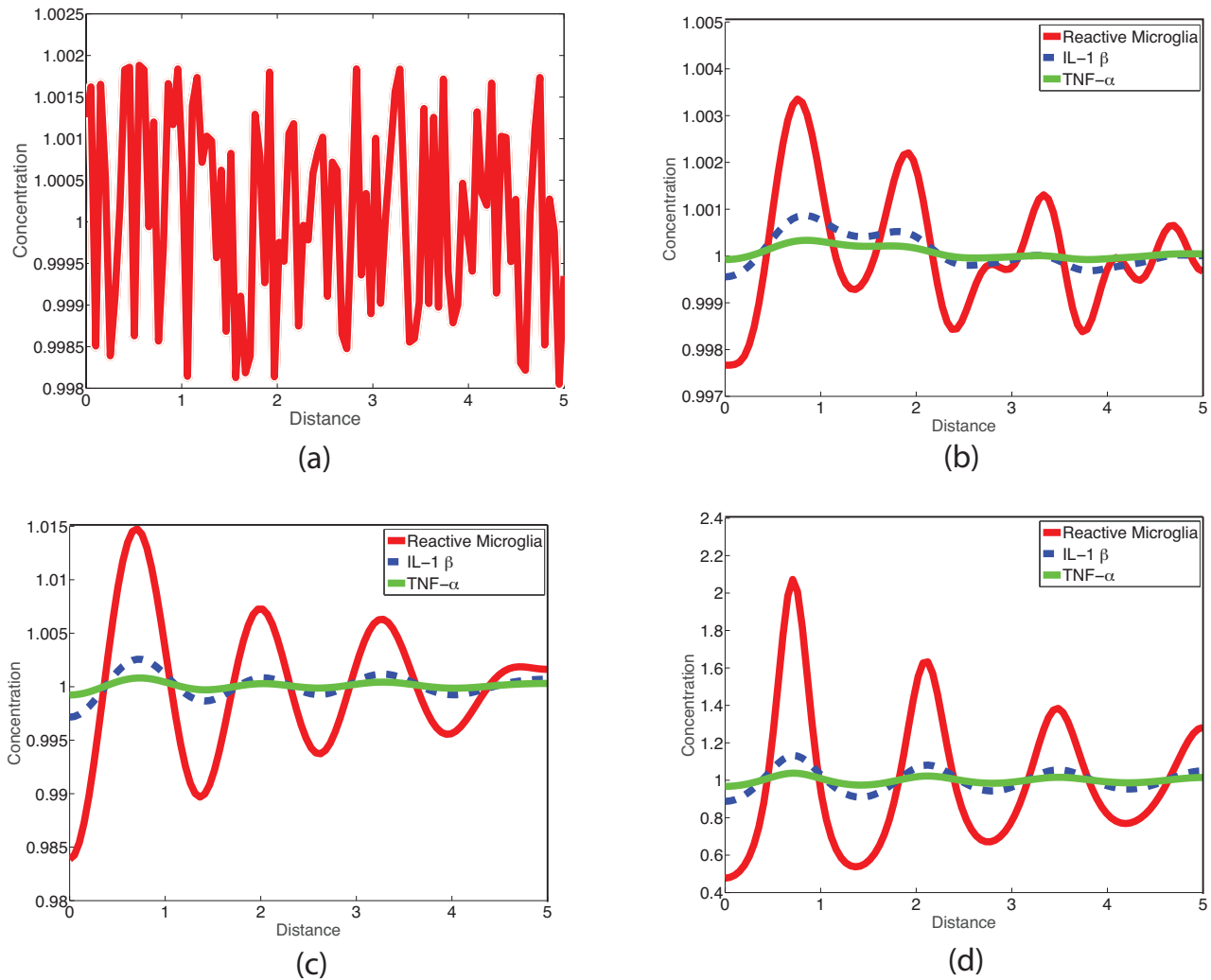


Figure 1: Concentration of reactive microglia, chemoattractant, and chemorepellent over space at (a) $t = 0$, (b) $t = 0.03$, (c) $t = 0.25$, (d) $t = 0.70$.

the pixel intensity profile overlaid onto the results from the chemotaxis model over a wider spatial region. We offset the beginning of the pixel intensity profile from the origin such that the data corresponds to the beginning of a cluster predicted by (3), thus enabling a comparison between the width of the microglia cluster observed in a PD brain and the predicted cluster from (3). The chemotaxis model predicts too wide of clusters of microglia.

A constraint of the chemotaxis model is the assumption of a constant amount of reactive microglia over time. Normal microglia revert to their reactive form in the presence of foreign bodies [12], and thus, in a dementia brain, we expect reactive microglia to proliferate with the aggregation of $A\beta$. We examine the proliferation of reactive microglia and its influences on the concentration.

3 Proliferation Model

Puri and Li [23] describe the relationships among the amount of $A\beta$, neurons, astrocytes, and microglia using a system of seven coupled, ordinary differential equations (6). Each equation describes the rate of change of number of cells over time. Variables are assumed to exist as one of two distinct states. That is, neurons exist either as surviving neurons (N_s) or dead neurons (N_d), astrocytes exist either as proliferating (A_p) or quiescent (A_q), and microglia exist either as normal (M_n) or reactive (M_r). The cells found predominately in a healthy brain are N_s , A_q , and M_n , and the cells found in a diseased brain are N_d , A_p , M_r , and $A\beta$. The total amount of each cell type remains constant over time; however, the proportion of

the variable in each state may change. For example, the total number of reactive microglia plus normal microglia remains constant over time, but the proportion of normal to reactive microglia varies over time. This assumption allows normal microglia to become reactive in response to $A\beta$, while retaining a constant total amount of microglia. In addition, the equations describing the number of cells found in an AD brain are the negated equations describing the corresponding healthy cells. For example, the equation describing reactive microglia, Equation 6f, is the negated version of the equation describing normal microglia, Equation 6e, meaning when the number of reactive microglia increase, the number of normal microglia decrease at the same rate. The normal microglia equation features the largest number of interactions among other variables, including $A\beta$. The variables are scaled by rates, denoted α_i , with the units 1/year.

$$\frac{dN_s}{dt} = \alpha_1 A_q - \alpha_2 A_p - \alpha_3 M_r, \tag{6a}$$

$$\frac{dN_d}{dt} = -\frac{dN_s}{dt}, \tag{6b}$$

$$\frac{dA_q}{dt} = \alpha_4 M_n - \alpha_5 M_r, \tag{6c}$$

$$\frac{dA_p}{dt} = -\frac{A_q}{dt}, \tag{6d}$$

$$\begin{aligned} \frac{dM_n}{dt} = & (\alpha_6 + \alpha_{11})N_s - \alpha_{10}N_d + (\alpha_7 + \alpha_{12})A_q \\ & - \alpha_9 M_r + \alpha_{14}M_n - (\alpha_8 + \alpha_{13})A\beta, \end{aligned} \tag{6e}$$

$$\frac{dM_r}{dt} = -\frac{dM_n}{dt}, \tag{6f}$$

$$\frac{dA\beta}{dt} = \alpha_{15}N_s - \alpha_{16}M_n \tag{6g}$$

The parameters used in the proliferation model (6), denoted by α_i , are defined in Table 3, and the initial conditions are defined in Table 4. These values are not based on clinical data.

We solve the proliferation model (6) using the ODE45 solver in MATLAB and Figure 3 shows the number of cells of microglia, astrocytes, neurons and $A\beta$ over time. We observe a slow rate of exponential growth for the number of reactive microglia cells in response to the aggregation of $A\beta$. The number of surviving neurons decreases as the $A\beta$ and reactive microglia populations increase. The amount of surviving neurons becomes smaller than the reactive microglia population around 10–12 years, which may correlate to symptomatic onset that usually occurs in AD patients around 17 years [29]. This observation suggests that symptomatic onset may begin after reactive microglia are more prevalent than surviving neurons in the brain. We assume a constant amount of total microglia, meaning that the sum of the amount of reactive microglia and normal microglia is constant over time. Thus, the

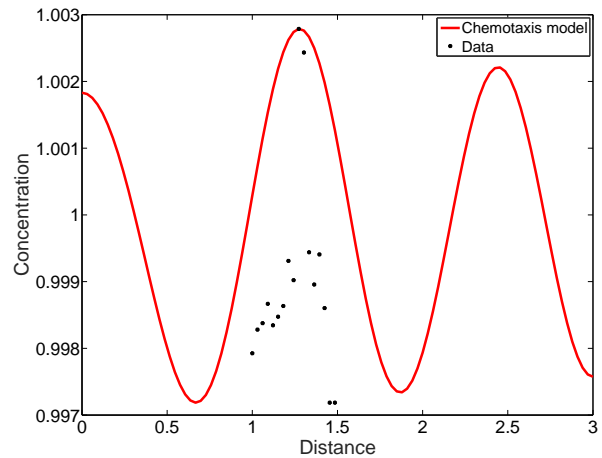


Figure 2: Predicted concentration of reactive microglia cells at $t = 0.10$ by the chemotaxis model compared to the pixel intensity profile of microglia clusters in a PD brain.

Parameter	α_1	α_2	α_3	α_4	α_5	α_6
Value	10^{-5}	10^{-3}	10^{-2}	10^{-4}	10^{-2}	10^{-2}
Parameter	α_7	α_8	α_9	α_{10}	α_{11}	α_{12}
Value	10^{-4}	10^{-2}	10^{-2}	10^{-2}	10^{-2}	10^{-4}
Parameter	α_{13}	α_{14}	α_{15}	α_{16}		
Value	10^{-2}	10^{-4}	1	10^{-2}		

Table 3: Parameter values used in the proliferation model (6) from [23].

Variable	$N_s(0)$	$N_d(0)$	$A_q(0)$	$A_p(0)$
Initial condition	10^4	10^2	10^5	10^3
Variable	$M_r(0)$	$M_n(0)$	$A\beta(0)$	
Initial condition	10^3	10^5	10^3	

Table 4: Initial conditions used in the proliferation model (6) from [23].

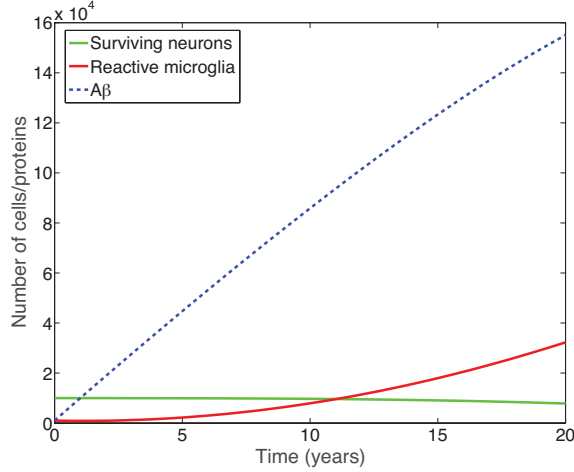


Figure 3: Number of surviving neuron, reactive microglia, and amyloid-beta cells over a 20-year span.

exponential growth of reactive microglia in Figure 3 indicates that normal microglial cells revert to their reactive state as $A\beta$ aggregates. We refer to this increase in reactive microglial cells as reactive microglia proliferation.

4 Chemotaxis Model with Proliferation

We incorporate the proliferation of reactive microglia using (6), into the chemotaxis model (3) to better predict reactive microglia behavior in response to $A\beta$. Luca et. al. [15] assume that proliferation of reactive microglia is inconsequential; however, results from the proliferation model (6) indicate reactive microglia proliferate up to 15% per year, coinciding with $A\beta$ aggregation.

We nondimensionalize the proliferation model (6) using the dimensionless variables defined in (2). We use \hat{m} to nondimensionalize all cell type variables N_s , N_d , A_q , A_p , M_r , M_n , and $A\beta$, and \hat{t} to nondimensionalize the time variable, t . The dimensionless variables are represented with stars.

$$\begin{aligned} N_s^* &= \frac{N_s}{\hat{m}}, & N_d^* &= \frac{N_d}{\hat{m}}, & A_q^* &= \frac{A_q}{\hat{m}}, & A_p^* &= \frac{A_p}{\hat{m}}, \\ M_r^* &= \frac{M_r}{\hat{m}}, & M_n^* &= \frac{M_n}{\hat{m}}, & A\beta^* &= \frac{A\beta}{\hat{m}}, & t^* &= \frac{t}{\hat{t}} \end{aligned} \quad (7)$$

We represent the addition of the proliferated reactive microglia by

$$\Delta M_r(x, t), \quad (8)$$

corresponding to Equation (6f).

Substituting the variables in (7) into the proliferation model (6), dropping the stars, and incorporating prolifer-

ated reactive microglia (8) into the predicted concentration of reactive microglia (3a) we obtain the chemotaxis model with proliferation

$$\frac{dN_s}{dt} = \hat{t}(\alpha_1 A_q - \alpha_2 A_p - \alpha_3 M_r), \quad (9a)$$

$$\frac{dN_d}{dt} = -\frac{dN_s}{dt}, \quad (9b)$$

$$\frac{dA_q}{dt} = \hat{t}(\alpha_4 M_n - \alpha_5 M_r), \quad (9c)$$

$$\frac{dA_p}{dt} = -\frac{A_q}{dt}, \quad (9d)$$

$$\begin{aligned} \frac{dM_n}{dt} &= \hat{t}((\alpha_6 + \alpha_{11})N_s - \alpha_{10}N_d + (\alpha_7 + \alpha_{12})A_q \\ &\quad - \alpha_9 M_r + \alpha_{14}M_n - (\alpha_8 + \alpha_{13})A\beta), \end{aligned} \quad (9e)$$

$$\frac{dM_r}{dt} = -\frac{dM_n}{dt}, \quad (9f)$$

$$\frac{dA\beta}{dt} = \hat{t}(\alpha_{15}N_s - \alpha_{16}M_n) \quad (9g)$$

$$\begin{aligned} \frac{\partial m}{\partial t} &= \frac{\partial^2 m}{\partial x^2} - \frac{\partial}{\partial x}((A_1 \frac{\partial c_1}{\partial x} - A_2 \frac{\partial c_2}{\partial x})m) + \Delta M_r(x, t), \end{aligned} \quad (9h)$$

$$\epsilon_1 \frac{\partial c_1}{\partial t} = \frac{\partial^2 c_1}{\partial x^2} + a^2(m - c_1), \quad (9i)$$

$$\epsilon_2 \frac{\partial c_2}{\partial t} = \frac{\partial^2 c_2}{\partial x^2} + m - c_2. \quad (9j)$$

The system is partially decoupled, with Equation 9h reflecting the coupling of the systems. Equation 9h incorporates the change in proliferation of reactive microglia predicted by the proliferation model, Equation 6f. We consider a uniform distribution of microglia proliferation and determine the equality

$$\Delta M_r(x, t) = \frac{\frac{dM_r}{dt}}{xLen} \quad (10)$$

In §4.4 we also consider a nonuniform distribution of proliferating microglia, where (8) is a non-constant function depending on time, t , and spatial location, x .

The chemotaxis model with proliferation (9) requires initial conditions of both total amount and spatial concentration of the reactive microglia. In order to ensure this agreement, we create the random spatial initial conditions for m , c_1 , and c_2 and then determine the initial conditions for the reactive microglia by summing the number of reactive microglia cells over the spatial region. We use (4) to define the initial conditions for the chemotaxis model variables, m , c_1 , and c_2 . We modify the initial condition for the concentration of reactive microglia in the chemotaxis model, (4), to determine the initial condition for the number of reactive microglia cells (M_r) in the proliferation model. We assume the brain is shaped like a cube as

we define the initial conditions. The modified condition

$$\sum_{i=0}^N (m(x_i, 0)) * xLen^3 \quad (11)$$

is multiplied by $xLen^3$ to convert from a concentration to the number of reactive microglia cells at each spatial step. The summation determines the total number of reactive microglia cells over the spatial region, where $x_0 = 0$ and $x_N = xLen$. We use the values in Table 4 for the initial conditions for the variables N_s , N_d , A_q , A_p , M_n , and $A\beta$.

4.1 Numerical Methods

To solve the chemotaxis model with proliferation (9), we first solve (9a–g) for $0 \leq t \leq 1$ using the ODE45 solver in MATLAB to determine the number of reactive microglia over time. We calculate the proliferation of reactive microglia cells over t using (10). We then use the PDEPE solver in MATLAB to solve (9h–j). At each time step, we incorporate the corresponding concentration of proliferated microglia into (9h).

4.2 Uniform Proliferation Results

We compare the microglia concentration predictions of the chemotaxis model with uniform proliferation (9), and the chemotaxis model (3) using the same initial conditions. Figure 4 shows the results at $t = 0.06, 0.45, 0.70$, where the blue lines represent the microglia concentration predictions from the chemotaxis model (3) and the red lines represent the microglia concentration predictions from the chemotaxis model with uniform proliferation (9). Over time, both models form the three distinct peaks of microglia density predicted by Luca et. al. [15]. Initially the chemotaxis model with uniform proliferation has the same shape as the chemotaxis model, only shifted higher. However, over time the chemotaxis model with uniform proliferation creates peaks that are taller and narrower than the chemotaxis model. This corresponds to smaller, more concentrated clusters of microglia. The maximum concentration predicted by the chemotaxis model with uniform proliferation is higher than the maximum predicted by the chemotaxis model, indicating that the proliferation of microglia impacts both the density and shape of microglia clusters.

4.3 Uniform Proliferation Verification

We compare the results of the chemotaxis model with uniform proliferation (9) to the image of stained reactive microglia cells in a PD brain (Figure 4 from [17]). We use the same pixel intensity profile obtained in Figure 2, however, we normalize the pixel intensity profile to the minimum and maximum concentration predictions from

the chemotaxis model with proliferation (9); we retain the same nondimensionalized spatial scale.

Figure 5 shows the concentration of microglia from (9) with a uniform distribution of microglia proliferation at $t = 0.10$ compared to the normalized pixel intensity profile of reactive microglia cells in a PD brain. Again, we use $t = 0.10$ to examine microglia concentrations after the likely time of symptomatic onset [29]. We compare the chemotaxis model to the chemotaxis model with uniform proliferation. While the chemotaxis model with uniform proliferation predicts narrower, taller peaks compared to the chemotaxis model, observed in Figure 4, the peaks are still wider than the microglia cluster observed in Figure 4 from [17]. Note that the pixel intensity profile appears larger in concentration in Figure 5 than in Figure 2, again due to normalizing the pixel intensity profile to the maximum and minimum values of the models used to generate the microglia concentration predictions, (1) and (9), respectively.

4.4 Nonuniform Proliferation

In §4.3 we assume the proliferating reactive microglia are uniformly distributed. We now consider the impact of nonuniform proliferation of reactive microglia on its concentration. In a diseased brain, chemotactic chemicals are secreted by stimulated astrocytes, reactive microglia, and other cells [2, 20]. Amyloid- β plaques aggravate astrocytes and microglia [20, 9], prompting the production of chemotactic chemicals near $A\beta$ plaques. Thus, while we retain the overall concentration of proliferation predicted by (6), we assume the proliferation of reactive microglia occurs entirely on the edges of the clusters and is negligible in the center of a microglia cluster and in the areas between clusters. From Figure 4, we observe that for a given initial condition, the microglia clusters develop at constant spatial locations, but become more distinct as time progresses. This observation justifies retaining a constant location of microglia proliferation, which we assume occurs at the edges of the formed peaks. At each time step in solving (9), we distribute the proliferated reactive microglia along the edges of the clusters. For example, a nonuniform proliferation distribution is shown in Figure 6 for three time steps, $t = 0.03, 0.05, 0.10$.

We compare the results of the chemotaxis model with nonuniform proliferation (9) to the image of reactive microglia from a PD brain (Figure 4 from [17]), using the nonuniform proliferation distribution shown in Figure 6. We normalize the pixel intensity profile to the minimum and maximum predicted concentrations from the chemotaxis model with nonuniform proliferation (9). Figure 7 compares the predictions from the chemotaxis model with nonuniform proliferation at $t = 0.10$ to the pixel intensity profile of reactive microglia in a PD brain. The nonuni-

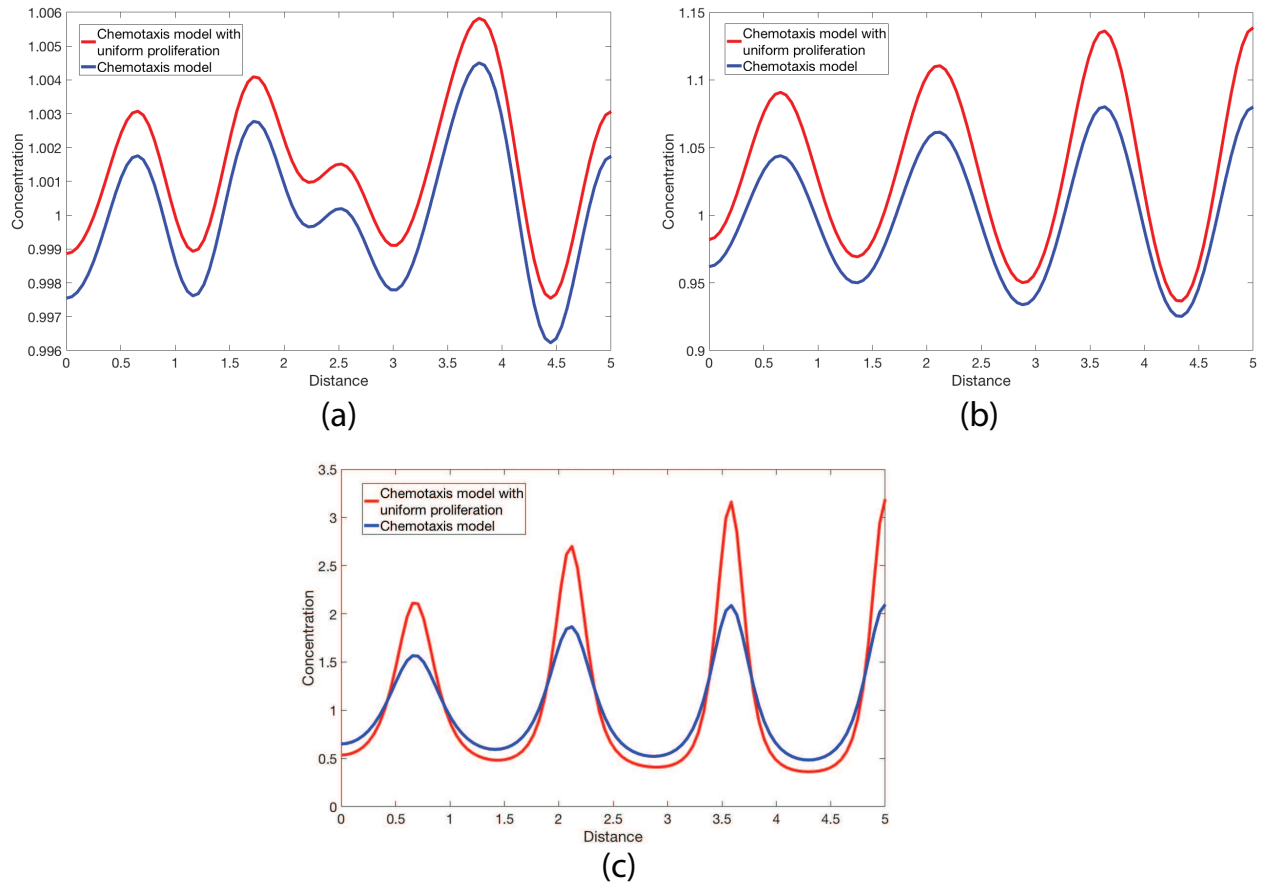


Figure 4: Concentration of reactive microglia predicted by the chemotaxis model with uniform proliferation and by the chemotaxis model over space at (a) $t = 0.06$, (b) $t = 0.45$, (c) $t = 0.70$.

form distribution of reactive microglia proliferation increases the number of microglia clusters predicted by the chemotaxis model with proliferation (9) and decreases the width of the formed microglia clusters. The chemotaxis model with nonuniform proliferation successfully predicts a narrower microglia cluster width that corresponds more applicably to the profile observed in the PD brain. The predicted concentration values of microglia clusters were higher using the model for nonuniform proliferation than in previous models, and we suggest this increase in predicted microglia concentration is due to incorporating large amounts of microglia into targeted areas of the brain (Figure 6), rather than incorporating smaller amounts of microglia uniformly distributed throughout the spatial scale, as observed with the uniform proliferation model. Note that we incorporate an equal amount of increasing microglia in both the uniform proliferation model and the nonuniform proliferation model, and change only the distribution of the increasing amounts of microglia.

With the parameter values in Table 2, Luca et. al. [15]

determined the chemotaxis model to be stable. Incorporating uniform distributions of proliferating microglia maintains the same wavenumber as that predicted in [15]. However, with the nonuniform microglia proliferation function shown in Figure 6, we double the number of predicted peaks. In all cases, the initial condition changes the predicted spatial location of the peaks and the height of the peaks, but will not alter the number of peaks observed. The variability in initial conditions alters the chosen spatial region of the models, equations (3) and (9), used to compare to the pixel intensity profile of microglia in a deceased PD brain. We shift the PD brain data to begin at the first full predicted microglia cluster, and this location changes depending on the initial condition used.

5 Discussion

The formation of amyloid-beta plaques is a hallmark of dementia, effectively disrupting the communication of

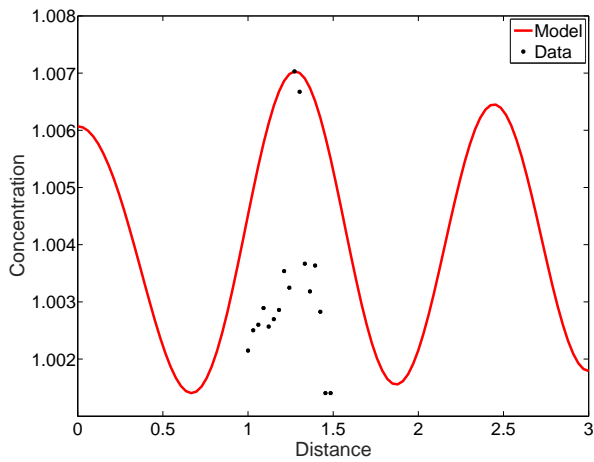


Figure 5: The reactive microglia cluster predictions of the chemotaxis model with uniform proliferation of reactive microglia at $t = 0.10$ compared to the pixel intensity profile of reactive microglia in a PD brain.

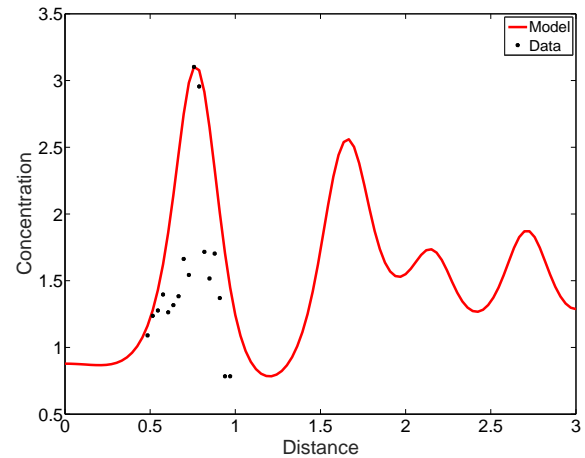


Figure 7: The reactive microglia cluster predictions of the chemotaxis model with nonuniform proliferation of reactive microglia at $t = 0.10$ compared to the pixel intensity profile of reactive microglia in a PD brain.

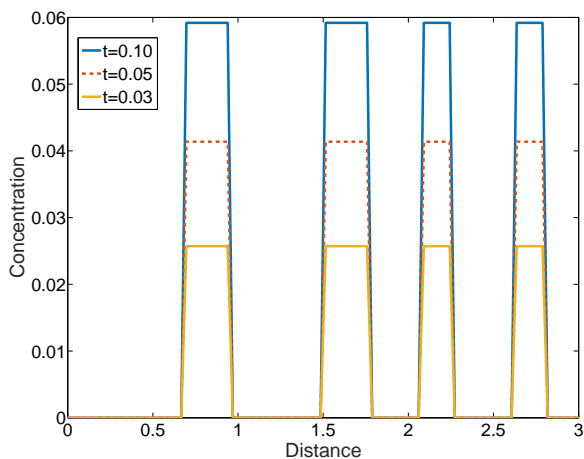


Figure 6: The nonuniform proliferation of reactive microglia at $t = 0.03, 0.05, 0.10$.

neurons [1]. However, measuring $A\beta$ is a difficult task but tracking microglial cells is more manageable. Using the assumption that microglia will cluster around $A\beta$ plaques, we focus on the location of the microglia. According to [23], as dementia progresses, the number of reactive microglia increases due to proliferation. Previously, the chemotactic behavior of microglia was examined in [15] [5], however, these studies assumed the number of reactive microglia remained constant. Incorporating the effects of an increasing number of microglia suggests that clusters of microglia will be more concentrated, better targeting the $A\beta$ plaques. Under the assumption that normal microglia near high concentrations of reactive microglia are more likely to switch to the reactive state, the robust results of the mathematical model suggest a good description of the cluster location in comparison to pictures of a PD brain.

While these results provide stronger support for the influences of chemotactic signaling in the progression of dementia, more experimental results are needed. The parameters used to model the crosstalk of the various cells were not reliant on experimental data. This portion of the model still needs to be validated as an accurate description of the change in number in each classification for the cell types. Additionally, values for the concentration of the microglia clusters would allow a more accurate comparison with the model, rather than being limited to the location and width of the microglia clusters. This study focused exclusively on a one dimensional description of the cell clusters. In order to be more realistic, the model must be expanded and verified in, ideally 3 dimensions. However, the limited data available is restricted to

2 dimensions.

A limitation of the chemotaxis model with proliferation is that the strength of the attraction and repulsion may change as the disease progresses, suggesting the need for a temporal influence on these parameters. In addition, we have assumed that the number of each type of cells is independent of the density of those cells. A future direction of this work is to integrate the influence of the density of the cells to the survival of neurons, thus impacting the number of cells present. Despite these limitations, a focused presence of an increasing number of microglia supports the need to further experimentally explore the role chemotactic signaling plays in the creation of plaques, which lead to degeneration of neurons.

References

- [1] ALZHEIMER'S ASSOCIATION, Alzheimer's Association Report: 2015 Alzheimer's disease facts and figures, *Alzheimer's Dement.*, 11(2015), pp. 332–384.
- [2] BENVENISTE, E. N., Cytokine production, in *Neuroglia*, H. Kettenmann and B. R. Ransom, eds., Oxford University Press, New York, 1995, pp. 700–713.
- [3] BRAAK, H. and K. D. TREDICI, Alzheimer's disease: Pathogenesis and prevention, *Alzheimer's Dement.*, 8(2012), pp. 227–233.
- [4] DAVIS, J. B., H. F. MCMURRAY, and D. SCHUBERT, The amyloid beta-protein of Alzheimer's disease is chemotactic for mononuclear phagocytes, *Biochem. Biophys. Res. Commun.*, 189(1992), pp. 1096–1100.
- [5] EDELSTEIN-KESHET, L. and A. SPIROS, Exploring the formation of Alzheimer's disease senile plaques in silico, *J. Theor. Biol.* 216(2002), pp. 301–326.
- [6] EROGLU, C. and B. A. BARRES, Regulation of synaptic connectivity by glia, *Nature*, 468(2010), pp. 223–231.
- [7] FARRELL, B., DANIELE LAUFFENBURGER, and D. LAUFFENBURGER, Quantitative relationships between single-cell and cell-population model parameters for chemosensory migration responses of alveolar macrophages to C5a, *Cell Motil. Cytoskeleton*, 16(1990), pp. 279–293.
- [8] IRWIN, D. J., V. M. LEE, and J. Q. TROJANOWSKI, Parkinson's disease dementia: convergence of α -synuclein, tau and amyloid- β pathologies, *Nat Rev Neurosci.*, 14(2013), pp. 626–36.
- [9] ITAGAKI, S., P. L. MCGEER, H. AKIYAMA, S. ZHU, and D. SELKOE, Relationship of microglia and astrocytes to amyloid deposits of Alzheimer's disease, *J. Neuroimmunol.*, 24(1989), pp. 173–182.
- [10] KOWALL, N. W. Beta amyloid neurotoxicity and neuronal degeneration in Alzheimer's disease, *Neurobiol. Aging*, 15(1994), pp. 257–258.
- [11] KRABBE, G., A. HALLE, V. MATYASH, J. L. RINNENTHAL, G. D. EOM, U. BERNHARDT, K. R. MILLER, S. PROKOP, H. KETTENMANN, and F. L. KEPPNER, Functional Impairment of Microglia Coincides with β -Amyloid Deposition in Mice with Alzheimer-Like Pathology, *PLoS ONE*, 8(2013).
- [12] KRYTSOS, C. R. Of Mice and Math: A Systems Biology Model for Alzheimer's Disease, University of Maryland, 2011.
- [13] KYRTSOS, C. R., and J. S. BARAS, Modeling the Role of the Glymphatic Pathway and Cerebral Blood Vessel Properties in Alzheimer's Disease Pathogenesis, *PLoS ONE* (2015).
- [14] LEE, S., W. LIE, D. DICKSON, C. BROSNAN and J. BERMAN, Cytokine production by human fetal microglia and astrocytes. Differential induction by lipopolysaccharide and IL-1, *Immunol.*, 150(1993), pp. 2659–2667.
- [15] LUCA, M., A. CHAVEZ-ROSS, L. EDELSTEIN-KESHET, and A. MOGILNER, Chemotactic Signaling, Microglia, and Alzheimer's Disease Senile Plaques: Is There a Connection?, *Bull Math Biol.*, 65(2003), pp. 693–730.
- [16] MACKENZIE, I. R., C. HAO, and D. G. MUNOZ, Role of microglia in senile plaque formation, *Neurobiol. Aging*, 16(1995), pp. 797–804.
- [17] MCGEER, P. L., S. ITAGAKI, B. E. BOYES, and E. G. MCGEER, Reactive microglia are positive for HLA-DR in the substantia nigra of Parkinson's and Alzheimer's disease brains, *Neurology*, 28(1988), pp. 1285–91.
- [18] MRAK, R. E., J. G. SHENG, and W. S. T. GRIFFIN, Glial cytokines in Alzheimer's disease: review and pathogenic implications, *Human Pathology* 26(1995), pp. 816–823.
- [19] MRAK, R. E., J. G. SHENG, and W. S. GRIFFIN, Glial cytokines in neurodegenerative conditions, in *Neuro-Immune Interactions in Neurologic and Psychiatric Disorders*, PATTERSON, KORDON, and CHRISTEN, eds., Springer, Berlin, 2000, pp. 9–17.

- [20] NILSSON, L., J. ROGERS, and H. POTTER, The essential role of inflammation and induced gene expression in the pathogenic pathway of Alzheimer's disease, *Front Biosci.*, 3(1998), pp. 436–446.
- [21] NOLTE, C., T. MOELLER, T. WALTER, and H. KETTENMANN, Complement 5a controls motility of murine microglial cells in vitro via activation of an inhibitory G-protein and the rearrangement of the actin cytoskeleton, *Neuroscience*, 73(1996), pp. 1091–1107.
- [22] NOLTE, C., F. KIRCHHOFF, and H. KETTENMANN, Epidermal growth factor is a motility factor for microglial cells in vitro: evidence for EGF receptor expression, *Eur. J. Neurosc.*, 9(1997), 1690–1698.
- [23] PURI, I. K., and L. LI, Mathematical Modeling for the Pathogenesis of Alzheimer's Disease, *PLoS ONE*, 5(2010).
- [24] SHENG, J. G., X. Q. ZHOU, R. E. MRAK, and W. S. T. GRIFFIN, Progressive neuronal injury associated with amyloid plaque formation in alzheimer disease, *J. Neuropathol. Exp. Neurol.*, 57(1998), pp. 714–717.
- [25] SMITS, H., L. A. BOVEN, C. PEREIRA, J. VERHOEF, and H. S. L. M. NOTTET, Role of macrophage activation in the pathogenesis of Alzheimer's disease and human immunodeficiency virus type I-associated dementia, *Eur. J. Clin. Invest.*, 30(2000), pp. 526–535.
- [26] STALDER, M., A. PHINNEY, A. PROBST, B. SOMMER, M. STAUFENBIEL, and M. JUCKER, Association of microglia with amyloid plaques in brains of APP23 transgenic mice, *Am. J. Pathol.*, 154(1999), pp. 1673–1684.
- [27] STREIT, W. J., and C. A. KINCAID-COLTON, The brain's immune system, *Sci Am.*, 273(1995), pp. 58–61.
- [28] ULLIAN, E. M., K. S. CHRISTOPHERSON, and B. A. BARRES, Role for glia in synaptogenesis, *Glia* 47(2004), pp. 209–216.
- [29] VILLEMAGNE, V. L., S. BURNHAM, P. BOURGEAT, B. BROWN, K. A. ELLIS, O. SALVADO, C. SZOEKE, S. L. MACAULAY, R. MARTINS, P. MARUFF, D. AMES, C. C. ROWE, and C. L. MASTERS, Amyloid- β deposition, neurodegeneration, and cognitive decline in sporadic Alzheimer's disease: a prospective cohort study, *Lancet Neurol.*, 12(2013), pp. 357–67.